SAND2023-07734C

A Practitioner's Guide to Local FRF Estimation

Keaton Coletti[1], Ryan Schultz[1], and Steven Carter[1]

[1]Sandia National Laboratories
Albuquerque, NM 87185

Abstract

Accurate measurement of frequency response functions is essential for system identification, model updating, and structural health monitoring. However, sensor noise and leakage cause variance and systematic errors in estimated FRFs. Low-noise sensors, windowing techniques, and intelligent experiment design can mitigate these effects but are often limited by practical considerations. This paper is a guide to implementation of local modeling methods for FRF estimation, which have been extensively researched but are seldom used in practice. Theoretical background is presented, and a procedure for automatically selecting a parameterization and model order is proposed. Computational improvements are discussed that make local modeling feasible for systems with many input and output channels. The methods discussed herein are validated on a simulation example and two experimental examples: a multi-input, multi-output system with three inputs and 84 outputs and a nonlinear beam assembly. They are shown to significantly outperform the traditional H_1 and H_{SVD} estimators.

Keywords: FRF estimation, local rational modeling, MIMO, non-parametric estimation, leakage

1 Introduction

Frequency response function (FRF) estimation is an essential step in characterization of dynamic systems. Traditional estimators, including the H_1, H_2, H_{SVD} (H_v), and $H_{SVD\text{-}2}$, are fast and easy to implement [1]. However, their noise rejection abilities are limited, and estimates are susceptible to leakage (also called transient) errors [8].

In recent years, local modeling techniques (also called nonparametric estimation) have been proposed in the literature [3,7,9,14]. Local modeling (LM) models the system FRF and transient in bands centered at each frequency of interest, which enables leakage removal and noise rejection. LM approaches generalize well to multi-input, multi-output (MIMO) systems, but they are significantly more difficult to implement and require additional user interaction. They are also more computationally expensive and can be prone to estimation instabilities and nonconvergence. This paper seeks to mitigate these shortcomings and to make next-generation FRF estimation accessible to the dynamics community.

Results included herein demonstrate that local modeling can significantly outperform traditional FRF estimation techniques. Outperformance includes large MIMO systems and highly nonlinear systems. Local modeling is especially useful when quality data is scarce or when leakage cannot be avoided. For example, in operational modal analysis, the analyst has little control over input signals, so windowing must be used to avoid excessive leakage errors [8]. However, windowing distorts measured data and affects modal parameter estimation [8]. In other cases, only short data records may be available. Even in a laboratory setting, averaging N panels (frames) of measured data or N impacts only reduces error as $\mathcal{O}(\sqrt{N})$. As a result, even the best measurement practices produce slow convergence, and removing noise is tedious. Local modeling can significantly reduce noise's impact on estimated FRFs.

Noise mitigation via averaging also sacrifices frequency resolution, which can be especially problematic near resonances. LM requires no averaging and generates FRFs with full frequency resolution. Without averaging, there is no need to, e.g., repeat random bursts, and a stationary random signal can be used. Without measuring free decay periods in each burst-random realization, the effective signal-to-noise ratio (SNR) is also increased.

In nonlinear testing, different input levels generate different nonlinear FRFs. In this case, averaging can be problematic. When conducting nonlinear characterization [11] using impact testing, it is thus helpful to generate high-quality FRFs from single impacts. LM enables this, eliminating the need for binning impacts by force level and averaging.

This paper is organized as follows. Section 2 presents a general theory of local modeling for MIMO systems and several parameterizations for the local models. Section 3 describes the computational approach used for local modeling and procedures for selecting a model and order. Section 4 demonstrates the approach's effectiveness on simulation data, and Section 5 demonstrates its effectiveness on a high-output MIMO system and on a nonlinear system subject to hammer excitation.

2 Theoretical Background

2.1 Problem formulation

Assume frequency-domain data (linear spectra) are available for a MIMO system with N_u input and N_y output channels, with $\mathbf{u}(\omega_k) \in \mathbb{C}^{N_u}$ as the input data and $\mathbf{y}(\omega_k) \in \mathbb{C}^{N_y}$ as the output data. These vectors are hereafter denoted $\mathbf{u}_k$ and $\mathbf{y}_k$ for each frequency bin ω_k. The input-output relationship for the measured data is given by

$$\mathbf{y}_k = \mathbf{H}_0(\boldsymbol{\theta})\,\mathbf{u}_k + \mathbf{t}_0(\boldsymbol{\theta}) + \boldsymbol{\varepsilon}_k. \tag{1}$$

Here $\mathbf{H}_0 \in \mathbb{C}^{N_y \times N_u}$ is the parameterized frequency response matrix (FRM) at ω_k, $\mathbf{t}_0$ is the parameterized transient (leakage) vector at ω_k, and $\boldsymbol{\varepsilon}$ is the error between modeled and measured response.

We seek to estimate $\mathbf{H}$ at each frequency bin via the parameter vector $\boldsymbol{\theta}$. Local modeling considers a band of width $N_b = 2R+1$ centered at ω_k, i.e., $\{\omega_{k-R}, \omega_{k-R+1}, \ldots, \omega_{k+R}\}$, and chooses $\boldsymbol{\theta}$ to minimize the error $\boldsymbol{\varepsilon}_{k+r}$ across the band, $-R \le r \le R$. Yuen showed that stationary time-domain random processes are independent and Gaussian in the freuqency domain [13]. Assuming known input and Gaussian output error yields

$$\begin{aligned}\hat{\boldsymbol{\theta}}_k &= \arg\min_{\boldsymbol{\theta}} \sum_{r=-R}^{R} \left|\left|\mathbf{y}_{k+r} - \mathbf{H}_r(\boldsymbol{\theta})\,\mathbf{u}_{k+r} - \mathbf{t}_r(\boldsymbol{\theta})\right|\right|^2, \\ &= \arg\min_{\boldsymbol{\theta}} f_k(\boldsymbol{\theta}).\end{aligned} \tag{2}$$

The estimated FRM $\hat{\mathbf{H}}_k$ at each frequency ω_k is given by $\mathbf{H}_0\left(\hat{\boldsymbol{\theta}}_k\right)$. To distinguish between output caused by the system input and by leakage, the frequency-domain input must be non-smooth [9], as is the case with random excitation. In the case of a smooth input source (e.g., impact testing), leakage is typically negligible, and estimation can proceed by setting $\mathbf{t}_r$ to $\mathbf{0}$.

2.2 Parameterizations

This section addresses the task of defining parameterizations $\mathbf{H}_r(\boldsymbol{\theta})$ and $\mathbf{t}_r(\boldsymbol{\theta})$. This paper uses the left matrix fraction description (MFD) [14],

$$\begin{aligned}\mathbf{H}_r(\boldsymbol{\theta}) &= \mathbf{D}_r^{-1}(\boldsymbol{\theta})\,\mathbf{A}_r(\boldsymbol{\theta}), \\ \mathbf{t}_r(\boldsymbol{\theta}) &= \mathbf{D}_r^{-1}(\boldsymbol{\theta})\,\mathbf{b}_r(\boldsymbol{\theta}).\end{aligned} \tag{3}$$

Voorhoeve presented several parameterizations of the denominator matrix $\mathbf{D}$ and FRF and transient numerator matrices $\mathbf{A}$ and $\mathbf{b}$ as functions of r [14]. Values p_d, p_a, and p_b represent the model order of $\mathbf{D}$, $\mathbf{A}$, and $\mathbf{b}$ respectively. The "Parsimonious" parameterization takes one order input, p. In the parameterizations below, the components d_s, $\boldsymbol{d}_s$, $\boldsymbol{D}_s$, $\boldsymbol{A}_s$, and $\boldsymbol{b}_s$ are direct rearrangements of the entries in $\boldsymbol{\theta}$. Denote by $\mathbf{I}_a$ the identity matrix in $\mathbb{R}^{a\times a}$.

Parameterization 1 (Common Denominator (CD))

$$\begin{aligned}\mathbf{D}_r(\boldsymbol{\theta}) &= \left(1 + \sum_{s=1}^{p_d} d_s(\boldsymbol{\theta}) r^s\right)\mathbf{I}_{N_y}, \quad d_s \in \mathbb{C}, \\ \mathbf{A}_r(\boldsymbol{\theta}) &= \sum_{s=0}^{p_a} \boldsymbol{A}_s(\boldsymbol{\theta}) r^s, \quad \boldsymbol{A}_s \in \mathbb{C}^{N_y \times N_u}, \\ \mathbf{b}_r(\boldsymbol{\theta}) &= \sum_{s=0}^{p_b} \boldsymbol{b}_s(\boldsymbol{\theta}) r^s, \quad \boldsymbol{b}_s \in \mathbb{C}^{N_y}.\end{aligned} \tag{4}$$

Parameterization 2 (Multi-input, single-output (MISO)) MISO is identical to the CD parameterization, except for the denominator matrix:

$$\mathbf{D}_r(\boldsymbol{\theta}) = 1 + \sum_{s=1}^{p_d} \left(\mathbf{I}_{N_y} \boldsymbol{d}_s(\boldsymbol{\theta})\right) r^s, \quad \boldsymbol{d}_s \in \mathbb{C}^{N_y}. \tag{5}$$

Parameterization 3 (Full MFD (FULL)) FULL is also identical to the CD and MISO parameterizations, except for the denominator matrix:

$$\mathbf{D}_r(\boldsymbol{\theta}) = 1 + \sum_{s=1}^{p_d} \boldsymbol{D}_s(\boldsymbol{\theta}) r^s, \quad \boldsymbol{D}_s \in \mathbb{C}^{N_y \times N_y}. \tag{6}$$

Parameterization 4 (Parsimonious (PARS))

$$\begin{aligned}
\mathbf{D}_r(\boldsymbol{\theta}) &= \begin{bmatrix} \mathbf{I}_l & 0 \\ \boldsymbol{D}_0 & \mathbf{I}_{N_y - l} \end{bmatrix} + \sum_{s=1}^{m-1} \boldsymbol{D}_s(\boldsymbol{\theta}) r^s + \begin{bmatrix} \boldsymbol{D}_m & \mathbf{0} \\ \mathbf{0} & \mathbf{0} \end{bmatrix} r^m, \quad \boldsymbol{D}_0 \in \mathbb{C}^{(N_y - l) \times l},\ \boldsymbol{D}_s \in \mathbb{C}^{Ny \times Ny},\ \boldsymbol{D}_m \in \mathbb{C}^{l \times l}, \\
\mathbf{A}_r(\boldsymbol{\theta}) &= \sum_{s=0}^{m-1} \boldsymbol{A}_s(\boldsymbol{\theta}) r^s + \begin{bmatrix} \boldsymbol{A}_m \\ \mathbf{0} \end{bmatrix}, \quad \boldsymbol{A}_s \in \mathbb{C}^{N_y \times N_u},\ \boldsymbol{A}_m \in \mathbb{C}^{l \times N_u}, \\
\mathbf{b}_r(\boldsymbol{\theta}) &= \sum_{s=0}^{m-1} \boldsymbol{b}_s(\boldsymbol{\theta}) r^s + \begin{bmatrix} \boldsymbol{b}_m \\ \mathbf{0} \end{bmatrix}, \quad \boldsymbol{b}_s \in \mathbb{C}^{N_y},\ \boldsymbol{b}_m \in \mathbb{C}^{l}, \\
m &= \left\lceil \frac{p}{N_y} \right\rceil, \ l = p - N_y(1 - m).
\end{aligned} \tag{7}$$

Table 1 gives the number of parameters, N_p, to estimate for each model as a function of N_u, N_y, and the model-order parameters.

Model	N_p, transient	N_p, no transient
CD	$p_d + N_y N_u\, p_a + N_y\, p_b + N_y\,(N_u + 1)$	$p_d + N_y N_u\, p_a + N_y\,(N_u + 1)$
MISO	$N_y\, p_d + N_y N_u\, p_a + N_y\, p_b + N_y\,(N_u + 1)$	$N_y\, p_d + N_y N_u\, p_a + N_y\,(N_u + 1)$
FULL	$N_y N_u\, p_d + N_y N_u\, p_a + N_y\, p_b + N_y\,(N_u + 1)$	$N_y N_u\, p_d + N_y N_u\, p_a + N_y\,(N_u + 1)$
PARS	$(N_u + N_y + 1)\, p + N_y\,(N_u + 1)$	$(N_u + N_y)\, p + N_y\,(N_u)$

Table 1: Number of parameters to estimate for each parameterization with and without transient (leakage) removal.

2.3 Model Selection

Selection of an appropriate model (parameterization and order) is critical to avoid underfitting or overfitting. Model selection is a major area of Bayesian research [12], and practical implementation requires a selection criterion that is not too computationally demanding. A modified minimum description length (MDL) criterion has been proposed by [9] for complex regression. It is expressed as

$$\frac{f_k\left(\hat{\boldsymbol{\theta}}_k\right)}{N_b - N_p} \exp\left(\frac{N_p \ln(2\, N_b)}{N_b - N_p - 2}\right). \tag{8}$$

At each frequency, estimates are computed for each model in a candidate set. The model is selected that minimizes Eq. (8). Minimization requires computing the solution for each candidate model, which may be computationally prohibitive in some applications. In this case, the analyst may simply specify a single reasonable model. Section 3.3 gives rules of thumb for selecting a candidate set and for selection of a single model to yield acceptable results.

3 Computation

This section presents the computational approach used to estimate each $\hat{\boldsymbol{\theta}}_k$. Section 3.1 presents an iterative linear least-squares approach to estimation, and Section 3.2 describes a method for improving compute time for large MIMO systems. Sections 3.3 and 3.4 describe the process of selecting a model and estimation bandwidth.

3.1 Iterative linear least squares

Minimizing the objective function in Eq. (2) is a nonlinear least-squares problem. The matrices $\mathbf{D}_r$, $\mathbf{A}_r$, and $\mathbf{b}_r$ can each be described as a linear mapping of the parameter vector $\boldsymbol{\theta}$, but the inversion of the denominator matrices $\mathbf{D}_r$ introduces nonlinearity. If desired, gradient-descent approaches could be applied to estimate $\hat{\boldsymbol{\theta}}_k$. However, when the

number of input and ouput channels is high, the optimization dimensionality N_p can be large (Table 1). Nonlinear approaches are therefore susceptible to convergence to local minima, resulting in unreliable FRF estimates. Further, optimization must be performed in each discrete frequency bin of interest: hence, the computational cost of nonlinear optimization is unacceptable for many applications.

Sanathanan and Koerner (SK) proposed an iterative linear least-squares algorithm for problems of this form [10]. The estimate $\hat{\boldsymbol{\theta}}_k^n$ in iteration n is given by

$$\begin{aligned}\hat{\boldsymbol{\theta}}_k^n &= \arg\min_{\boldsymbol{\theta}} \sum_r \left|\left| \left[\mathbf{D}_r\left(\hat{\boldsymbol{\theta}}_k^{n-1}\right)\right]^{-1} \left(\mathbf{D}_r\left(\boldsymbol{\theta}\right)\mathbf{y}_{k+r} - \mathbf{A}_r\left(\boldsymbol{\theta}\right)\mathbf{u}_{k+r} - \mathbf{b}_r\left(\boldsymbol{\theta}\right)\right)\right|\right|^2 \\ &= \arg\min_{\boldsymbol{\theta}} \sum_r \left|\left|\mathbf{D}_r^{\mathrm{pr}}\left(\mathbf{X}_r\,\boldsymbol{\theta} + \mathbf{y}_{k+r}\right)\right|\right|^2 .\end{aligned} \tag{9}$$

Linear mappings $\mathbf{X}_r$ for each parameterization are provided in Table 2. For convenience, the following notation is used:

$$\mathbf{X}_r = \begin{bmatrix}\mathbf{M}_{r,1} & -\mathbf{M}_{r,2} & -\mathbf{M}_{r,3}\end{bmatrix}, \tag{10}$$

$$\left[\mathbf{r}\right]_a^b = \begin{bmatrix} r^a & r^{a+1} & \dots & r^b\end{bmatrix}, \tag{11}$$

$$\left[\mathbf{y}_r\right]^l = \mathbf{y}_{k+r}^T \begin{bmatrix}\mathbf{I}_l \\ \mathbf{0}\end{bmatrix}. \tag{12}$$

Minimization of Eq. (9) is computed in a single least-squares step by

$$\hat{\boldsymbol{\theta}}_k^n = \left[\mathbf{L}^n\right]^+ \mathbf{q}^n, \tag{13}$$

$$\mathbf{L}^n = \begin{bmatrix}\mathbf{D}_{k-R}^{\mathrm{pr}}\mathbf{X}_{k-R} \\ \mathbf{D}_{k-R+1}^{\mathrm{pr}}\mathbf{X}_{k-R+1} \\ \vdots \\ \mathbf{D}_{k+R}^{\mathrm{pr}}\mathbf{X}_{k+R}\end{bmatrix}, \quad \mathbf{q}^n = -\begin{bmatrix}\mathbf{D}_{k-R}^{\mathrm{pr}}\mathbf{y}_{k-R} \\ \mathbf{D}_{k-R+1}^{\mathrm{pr}}\mathbf{y}_{k-R+1} \\ \vdots \\ \mathbf{D}_{k+R}^{\mathrm{pr}}\mathbf{y}_{k+R}\end{bmatrix}, \tag{14}$$

where $(\circ)^+$ denotes the left pseudoinverse. Iterations continue until convergence is achieved or until a maximum iteration count is reached. Algorithm 1 presents a basic implementation that captures nonconvergence to enhace stability.

Algorithm 1 Sanathanan-Koerner linearized iterations

Initialize $\mathbf{D}_r^{\mathrm{pr}} = 1$, $\hat{\boldsymbol{\theta}}^{\mathrm{pr}} = \mathbf{0}$, $f^{\min} = \mathrm{Inf}$
Compute $\mathbf{X}_r$ from Table 2

for $n \in \{1, 2, \dots, N + N_{\mathrm{nc}}\}$ **do**
  Assemble $\mathbf{L}$ and $\mathbf{q}$
  Compute $\hat{\boldsymbol{\theta}} = \mathbf{L}^+\mathbf{q}$ ▷ Moore-Penrose pseudoinverse
  if $\left|\left|\left(\hat{\boldsymbol{\theta}} - \hat{\boldsymbol{\theta}}^{\mathrm{pr}}\right) \oslash \hat{\boldsymbol{\theta}}^{\mathrm{pr}}\right|\right|_\infty \leq$ threshold **then** ▷ check for convergence
    Set $\hat{\boldsymbol{\theta}}_k = \hat{\boldsymbol{\theta}}$
    Exit loop
  else
    Assign $\mathbf{D}_r^{\mathrm{pr}} = \left[\mathbf{D}_r\left(\hat{\boldsymbol{\theta}}\right)\right]^{-1}$
  end if
  if $n > N$ **then** ▷ protect against non-convergence
    if $f_k\left(\hat{\boldsymbol{\theta}}\right) < f^{\min}$ **then**
      Set $\hat{\boldsymbol{\theta}}_k = \hat{\boldsymbol{\theta}}$
      Set $f^{\min} = f_k\left(\hat{\boldsymbol{\theta}}\right)$
    end if
  end if
end for

Model	$\mathbf{M}_{1,r}$	$\mathbf{M}_{2,r}$	$\mathbf{M}_{3,r}$
CD	$\mathbf{y}_{k+r}\left[\mathbf{r}\right]_1^{p_d}$	$\left(\left[\mathbf{r}\right]_0^{p_a} \otimes \mathbf{u}_{k+r}^T\right) \otimes \mathbf{I}_{N_y}$	$\left[\mathbf{r}\right]_0^{p_b} \otimes \mathbf{I}_{N_y}$
MISO	$\left[\mathbf{r}\right]_1^{p_d} \otimes \mathrm{diag}\left(\mathbf{y}_{k+r}\right)$	$\left(\left[\mathbf{r}\right]_0^{p_a} \otimes \mathbf{u}_{k+r}^T\right) \otimes \mathbf{I}_{N_y}$	$\left[\mathbf{r}\right]_0^{p_b} \otimes \mathbf{I}_{N_y}$
FULL	$\left(\left[\mathbf{r}\right]_1^{p_d} \otimes \mathbf{y}_{k+r}^T\right) \otimes \mathbf{I}_{N_y}$	$\left(\left[\mathbf{r}\right]_0^{p_a} \otimes \mathbf{u}_{k+r}^T\right) \otimes \mathbf{I}_{N_y}$	$\left[\mathbf{r}\right]_0^{p_b} \otimes \mathbf{I}_{N_y}$
PARS	$\begin{bmatrix} \left[\mathbf{y}_r\right]^l \otimes \begin{bmatrix} \mathbf{0} \\ \mathbf{I}_{N_y-l} \end{bmatrix} & \left(\left[\mathbf{r}\right]_1^{m-1} \otimes \mathbf{y}_{k+r}^T\right) \otimes \mathbf{I}_{N_y} \\ & \cdots\ r^m \left[\mathbf{y}_r\right]^l \otimes \begin{bmatrix} \mathbf{I}_l \\ \mathbf{0} \end{bmatrix} \end{bmatrix}$	$\begin{bmatrix} \left(\left[\mathbf{r}\right]_0^{m-1} \otimes \mathbf{u}_{k+r}^T\right) \otimes \mathbf{I}_{N_y} \\ \cdots\ r^m \mathbf{u}_{k+r}^T \otimes \begin{bmatrix} \mathbf{I}_l \\ \mathbf{0} \end{bmatrix} \end{bmatrix}$	$\begin{bmatrix} \left[\mathbf{r}\right]_0^{m-1} \otimes \mathbf{I}_{N_y} & r^m \begin{bmatrix} \mathbf{I}_l \\ \mathbf{0} \end{bmatrix} \end{bmatrix}$

Table 2: Components of linearized matrices $\mathbf{X}_j$.

3.2 Reducing compute time for MISO configuration

In Eq. (13), $\mathbf{L}^n \in \mathbb{C}^{N_y N_b \times N_p}$. Table 1 shows that $N_p = \mathcal{O}\left(N_y\right)$ for large N_y. Hence, for many-output systems, $\mathbf{L}^n$ has $\mathcal{O}\left(N_y^2\right)$ elements. When the number of input channels, N_u, and the number of frequency bins in the local bandwith, N_b, are also large, calculating the pseudoinverse $\left[\mathbf{L}^n\right]^+$ dominates computation time. Because the SK procedure requires multiple iterations, and estimation of $\mathbf{H}_k$ is performed at each frequency bin ω_k, the linearized procedure becomes computationally prohibitive even when bins are computed in parallel.

However, inspection of Eq. (5) and the MISO row of Table 2 reveals that equations relating the inputs $\mathbf{u}$ to outputs $\mathbf{y}$ are uncoupled for the MISO configuration. Independence gives the option of computing each row of the frequency response matrix individually, which reduces the dimensionality of the pseudoinversion to $\mathbf{L}_j^n \in \mathbb{C}^{\mathcal{O}(1)}$ with $j = 1, 2, \ldots, N_y$. The FRM estimate at ω_k is then a concatenation of the single-output estimates,

$$\hat{\mathbf{H}}_k = \begin{bmatrix} \mathbf{H}_0\left(\hat{\boldsymbol{\theta}}_{k,1}\right) \\ \mathbf{H}_0\left(\hat{\boldsymbol{\theta}}_{k,2}\right) \\ \vdots \\ \mathbf{H}_0\left(\hat{\boldsymbol{\theta}}_{k,N_y}\right) \end{bmatrix} \tag{15}$$

The estimate $\hat{\boldsymbol{\theta}}_{k,j}^n$ in SK iteration n is

$$\hat{\boldsymbol{\theta}}_{k,j}^n = \left[\mathbf{L}_j^n\right]^+ \mathbf{q}_j^n, \tag{16}$$

where $\mathbf{L}_j^n$ and $\mathbf{q}_j^n$ are computed from Eq. (14) considering only output channel j. The least-squares solutions $\left[\mathbf{L}_j^n\right]^+ \mathbf{q}_j^n$ can be computed without loss of efficiency by, e.g., stacking as a 3-D array over j and using a commercial linear least-squares solver such as *pagemldivide* (MATLAB© 2023a).

The diagonal form of the MISO denominator matrices $\mathbf{D}_r$ also allows for element-wise inversion to produce the SK correction matrices $\mathbf{D}_{r,j}^{\mathrm{pr}}$. This enables partial assembly of $\mathbf{L}_j^n$ and $\mathbf{q}_j^n$ prior to the SK iterations and simple element-wise division to update them in each iteration.

3.3 Model selction rules of thumb

3.3.1 Automatic selection

In multi-output configurations, the MISO parameterization should be preferred due to its computational efficiency. For systems with fewer outputs, experience has shown that the CD and PARS parameterizations also generate acceptable results, but the FULL parameterization is prone to overfitting. Denote, e.g., a model consisting of the MISO parameterization with order $p_a = 1$, $p_b = 2$, and $p_d = 3$ by $\mathrm{MISO}\left(1, 2, 3\right)$.

Fig. 1 shows examples of automatic model selection on the linear ($N_u = 3$, $N_y = 84$) and nonlinear ($N_u = 1$, $N_y = 24$) systems discussed in Sections 5.1 and 5.2. The selection set used is MISO with $1 \leq p_a, p_b \leq 3$, $0 \leq p_d \leq 3$. Smoothing bandwidths are 20 Hz in both cases, and estimation is performed on five 4-second bursts and a single impact, respectively. Transient estimation is disabled for the impact tests. Denominator order tends to increase at

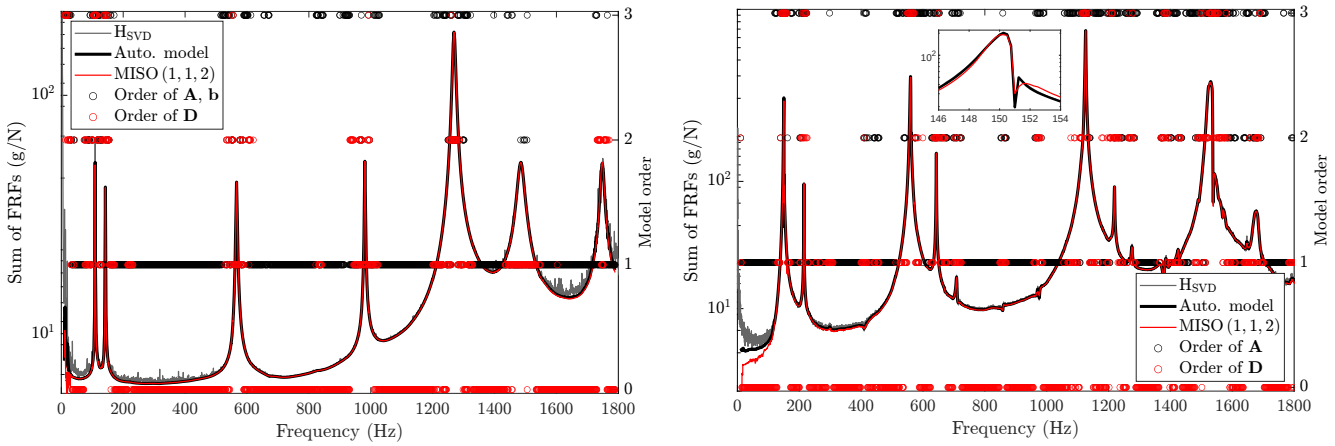

Figure 1: Application of model selection to (a) linear and (b) nonlinear systems. Scatter plots show the selected model order at each frequency bin analyzed (right axes), overlaid on the sum of all FRF magnitudes at each frequency (left axes). In (a), the candidate set includes only orders where $p_a = p_b$.

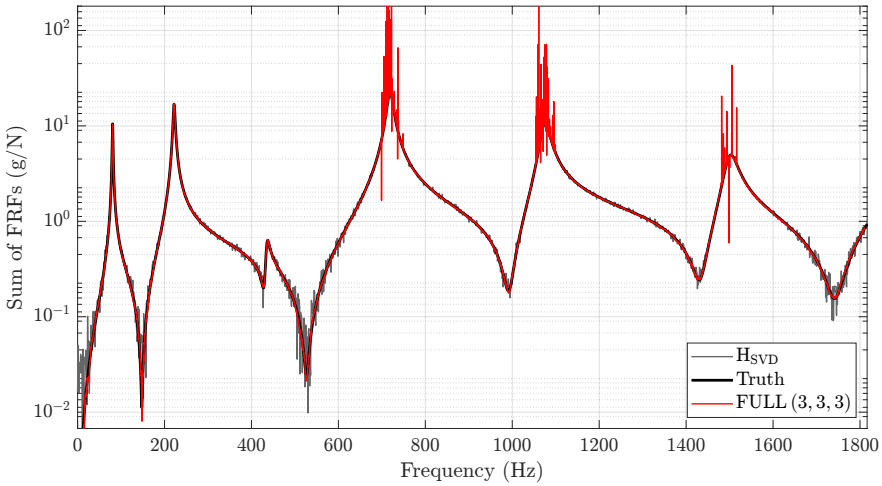

Figure 2: Example of overfitted FRF resulting from an excessive model order. This figure was generated by applying the FULL $(3, 3, 3)$ model with 10 Hz bandwidth to 10 seconds of random vibration from the simulation described in Section 4.

resonances, and numerator order increases in the high-slope regions on either side of the resonances. The selection procedure prefers higher model orders in the nonlinear case, where FRF geometry is more complicated.

3.3.2 Manual selection

When computation time is limited, best practice is to specify a small candidate set for automatic selection (e.g., $\{\text{MISO}\,(1,1,1)\,,\ \text{MISO}\,(2,2,2)\}$). However, intelligent selection of a single model can yield acceptable results. For linear systems, minimum model orders for sufficient description are typically $(1, 1, 0)$ at off-resonances and $(1, 1, 1)$ at resonances. For very lightly damped systems, selecting a model order that is too low results in underestimation of the resonance peaks [9]. In such cases, setting $p_d = 2$ can improve estimation. For nonlinear systems, complicated behavior near resonances may require higher model orders to resolve their behavior. The red plot in Fig. 1 shows sums of FRF magnitudes when selecting a single model. As can be seen in the zoomed portion of Fig. 1b, selecting $\text{MISO}\,(1, 1, 2)$ results in underfitting the nonlinear FRF.

When using manual selection, FRFs should be inspected for overfitting. An example is shown in Fig. 2. Overfitting yields larger errors than underfitting but can typically be identified by visual inspection of the estimated FRF.

3.4 Estimation bandwidth and step size

In the proposed formulation, the user selects the bandwith for local modeling. Larger bandwidths enhance noise removal but require higher model orders to adequately desribe system behavior. The bandwidth should be set as large as possible such that the candidate models can adequately describe FRF sctructure in each band. At minimum, stability requires $N_w\, N_y > N_p$ so that the least-squares problem in Eqs. (2) and (13) is overdetermined. McQuarrie suggested that $N_w\, N_y > 10\, N_p$ [5], but automatic model selection rejects overfitting, and experience shows that acceptable estimates are generated by $N_w\, N_y > 2\, N_p$, though the risk of instability increases. When automatic selection is used, the bandwidth should be set to satisfy these requirements for the largest model in the candidate set.

In many applications, computing FRFs at the full available frequency resolution is unnecessary. For example, a 40-second data record will generate a 0.025 Hz frequency bin width when a discrete Fourier transform is applied. With traditional approaches, this record might be paneled and averaged to yield a 1 Hz bin width. Local modeling still uses all the data but does so without averaging. If the analyst only desires a 1 Hz bin-width FRF, local modeling can be computed using 1/40 of the bins ($\Delta k = 40$) at significant computational gain. Another option is to model in bandwidths centered at a subset of ω_k but to apply the local models to every bin as

$$\hat{\mathbf{H}}_{k-\Delta k/2+1} = \mathbf{H}_{-\Delta k/2+1}\left(\hat{\boldsymbol{\theta}}_k\right), \ldots, \hat{\mathbf{H}}_{k+\Delta k/2} = \mathbf{H}_{\Delta k/2}\left(\hat{\boldsymbol{\theta}}_k\right). \tag{17}$$

An outline of the entire estimation process is provided in Algorithm 2.

Algorithm 2 Estimation outline

```
Compute linear spectra u(ω_k) ∈ ℂ^{N_u}, y(ω_k) ∈ ℂ^{N_y}
Select estimation bandwidth and calculate N_b = 2R + 1
Select a model candidate set (with or without transient)
Select step size Δk

for each frequency ω_{R+1}, ω_{R+1+Δk}, ... do
    for each candidate model M do
        Estimate θ̂_k^M using Algorighthm 1
        Compute MDL^M using Eq. (8)
    end for

    Select model M* with minimum MDL
    Assign Ĥ(ω_k) = H_0(θ̂_k^{M*})
end for
```

4 Simulation Demonstration

This section presents an application of local modeling to a simulation example, where the true FRM is known. The simulation structure is a free-free Euler-Bernoulli beam with length 1 m, width 10 cm, and thickness 15 mm. The density is 7700 kg/m^3, and the Young's modulus is 210 GPa. Bending mode shapes and natural frequencies are solved analytically [2], and response to arbitrary excitation is solved via modal space, time-domain integration using the Newmark-Beta algorithm. Excitation and response are synthesized at three input locations and six output locations along the beam length.

A stationary, uncorrelated, 10-second white-noise random input is simulated at the three input locations. Without additive noise, Fig. 3a shows that LM almost perfectly removes leakage effects that significantly affect the $\mathrm{H}_{\mathrm{SVD}}$ estimate. Fig. 3b gives an example where noise was added with a 30 dB input signal-to-noise ratio (SNR) and 40 dB output SNR. For convenience of viewing, only a two output, one input sample of the FRM is shown. The local model uses a 20 Hz estimation bandwidth and automatic selection from a candidate set including CD, MISO, and PARS with $1 \le p_a, p_b \le 2$, $0 \le p_d \le 2$, and $1 \le p \le 3$. $\mathrm{H}_{\mathrm{SVD}}$ estimates $[1, 6]$ are computed using ten rectangular windows (Fig. 3a) and ten Hanning windows (Fig. 3b). Modal damping is assumed 1% of critical damping for all modes.

In the presence of noise and leakage, local modeling yields better FRF estimates with far fewer data. Fig. 4 plots mean FRF error across all entries in the FRM versus length of simulated data record. The error metric used is the Modified Frequency Response Assurance Criterion (MFRAC), given by multiplying the FRAC by the ratio of

root-mean-square (RMS) values [4]. For a pair of single-input, single-output FRFs, H_A and H_B,

$$\text{MFRAC} = \frac{\min\{\text{RMS}_A, \text{RMS}_B\}}{\max\{\text{RMS}_A, \text{RMS}_B\}} \frac{\left|\sum_{\omega_k}\left(H_A(\omega_k)^H H_B(\omega_k)\right)\right|^2}{\sum_{\omega_k}\left(H_A(\omega_k)^H H_A(\omega_k)\right)\sum_{\omega_k}\left(H_B(\omega_k)^H H_B(\omega_k)\right)}. \tag{18}$$

In Fig. 4, data are simulated with 0.2% modal damping to demonstrate the ability to estimate lightly damped resonance peaks. A 20 Hz estimation bandwidth is used. The H_{SVD} estimates are computed using a number of Hanning windows equal to the data-record length in seconds, resulting in a 1 Hz bin width.

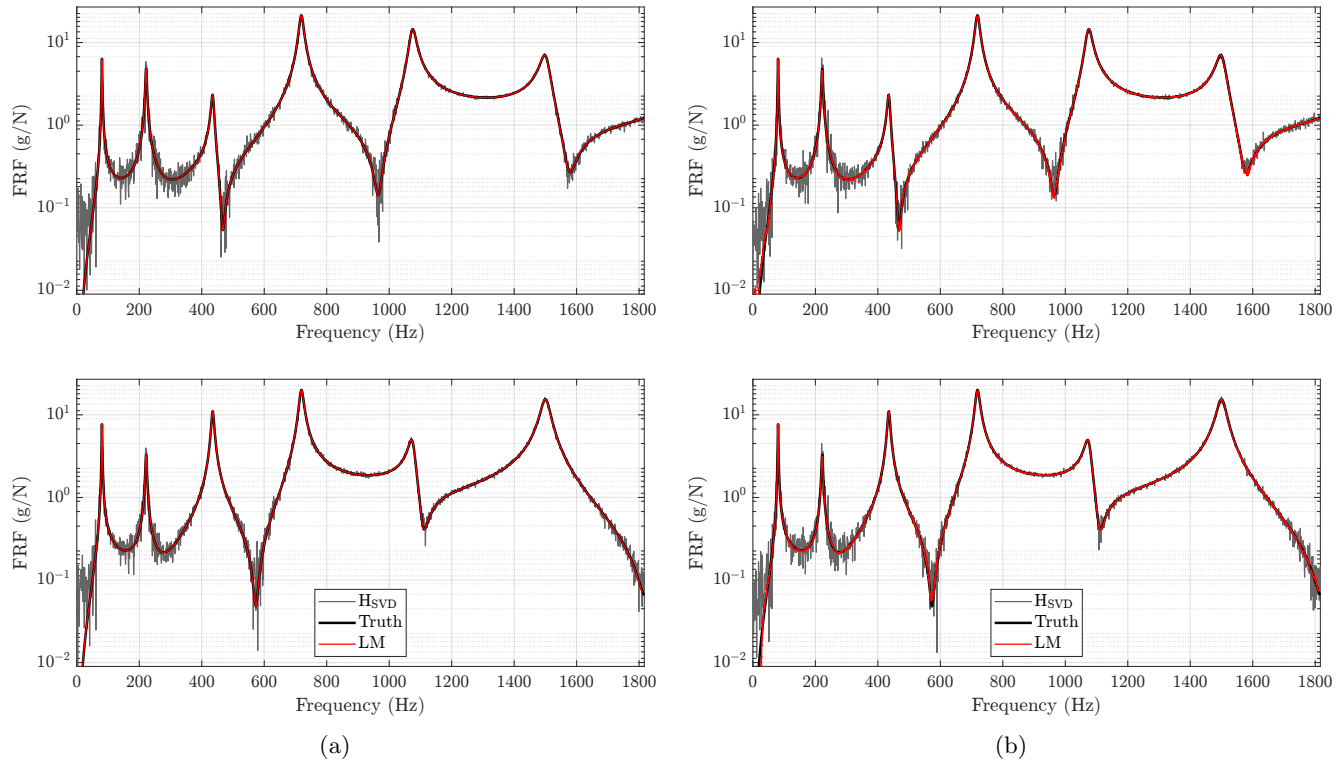

Figure 3: Demonstration of LM on a simulated Euler-Bernoulli beam with (a) no added noise and (b) 30 dB input SNR and 40 dB output SNR.

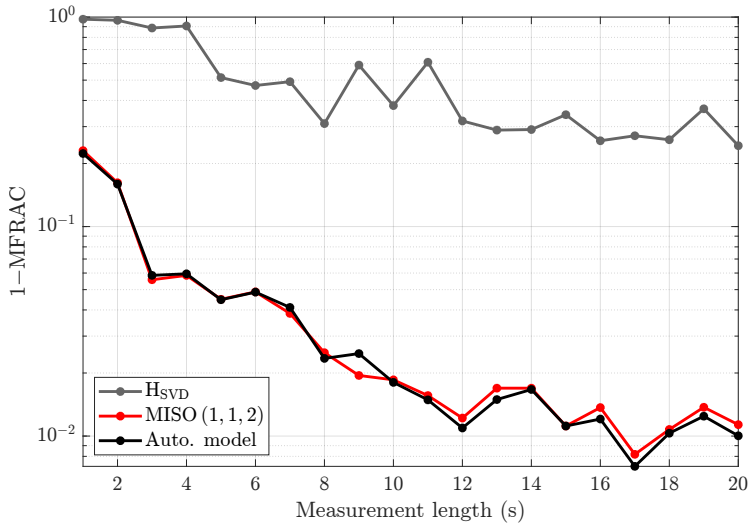

Figure 4: MFRAC performance of H_{SVD}, manual LM, and automatic LM approaches versus data record length for the simulation example with 0.2% modal damping.

5 Experimental Demonstration

This section presents two experimental validations of the proposed methods. Section 5.1 demonstrates LM capabilities on an approximately linear MIMO system subject to shaker excitation. Then, Section 5.2 demonstrates LM on impact testing of a nonlinear beam assembly.

5.1 High-output MIMO system

The system considered in this section is a cylinder assembly with an internal cantilevered beam and is pictured in Fig. 7. The structure is excited by three shakers instrumented with force gauges. Acceleration data is collected from 28 triaxial accelerometers at 5 kHz and 4.1 kHz sampling rates for stationary-random and burst-random trials, respectively. The "truth" FRM is estimated using $\mathrm{H}_{\mathrm{SVD}}$ on 144 repetitions of a 4-second random burst with 25% force-input duration.

Fig. 5 shows a 3×3 sample of the estimated FRM using $\mathrm{H}_{\mathrm{SVD}}$ and LM. Here, 15 seconds of random input with the measured force-covariance structure

$$\begin{bmatrix} 1.0 & 0.5e^{0.25\pi} & 0.5e^{0.12\pi} \\ 0.5e^{-0.25\pi} & 1.0 & 0.5e^{1.00\pi} \\ 0.5e^{-0.12\pi} & 0.5e^{-1.00\pi} & 1.0 \end{bmatrix} \tag{19}$$

at each frequency bin between 10 and 2000 Hz is used for estimation. Because this case features a truncated signal and correlated input structure, it represents a sub-optimal test configuration. $\mathrm{H}_{\mathrm{SVD}}$ is performed using 15 Hanning windows, and LM is performed using a 30 Hz bandwidth and automatic selection from the set $\{\text{MISO}, 1 \leq p_a, b_b \leq 2, 0 \leq p_d \leq 2\}$.

To demonstrate that local modeling improves FRF estimates even when best practices are used, this comparison is repeated on 15 4-second uncorrelated bursts. Local modeling is computed as in the previous example, and resulting estimates are shown in Fig. 6. With only 15 frames of data, the LM estimate appears superior to the $\mathrm{H}_{\mathrm{SVD}}$ estimate with 144 frames.

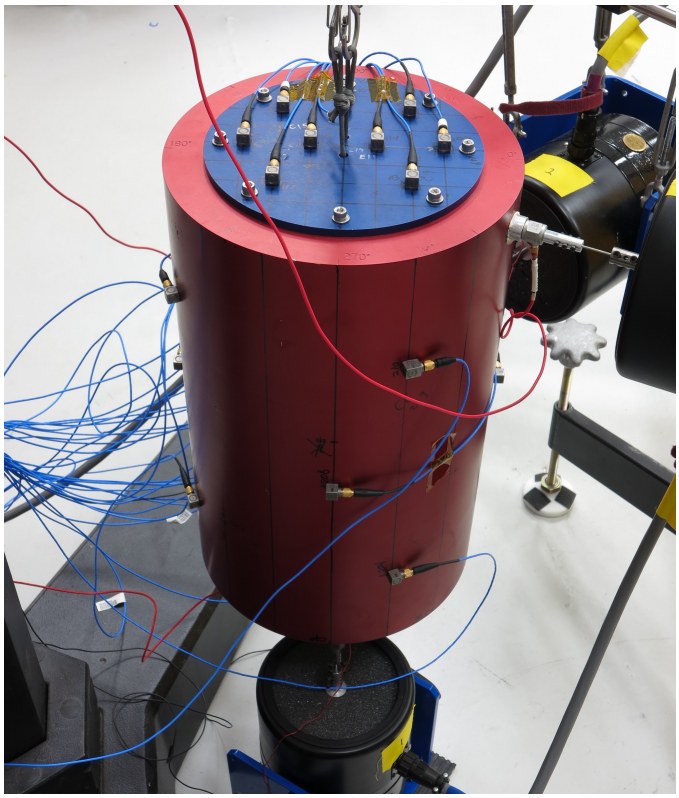

Figure 7: MIMO experiment setup.

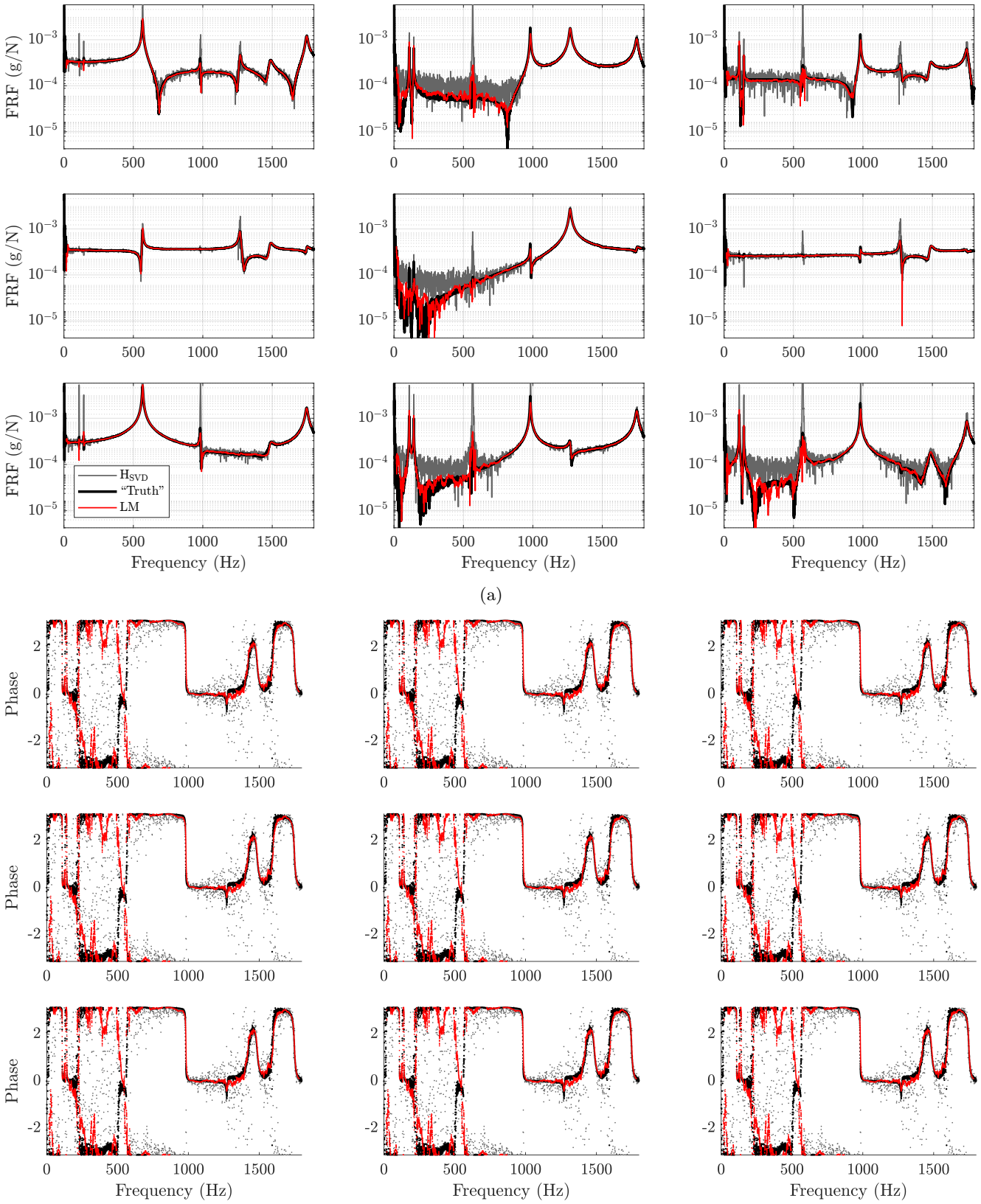

Figure 5: Estimated FRF (a) magnitude and (b) phase for a three-ouptut sample of the MIMO experimental confguration with 15 seconds of correlated-random input. MFRAC values for the entire FRM are 0.186 for H_{SVD} (gray) and 0.693 for LM (red) when compared with the "truth" estimate (black).

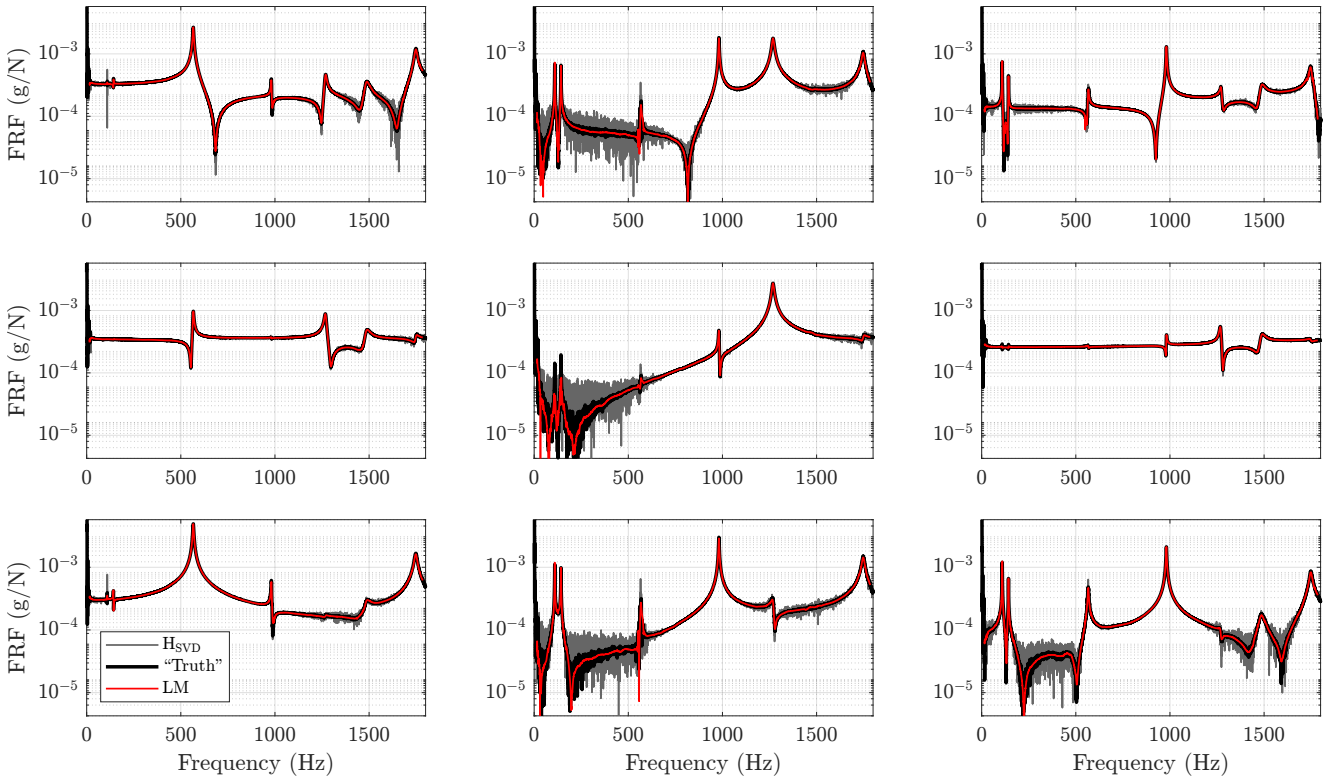

(a)

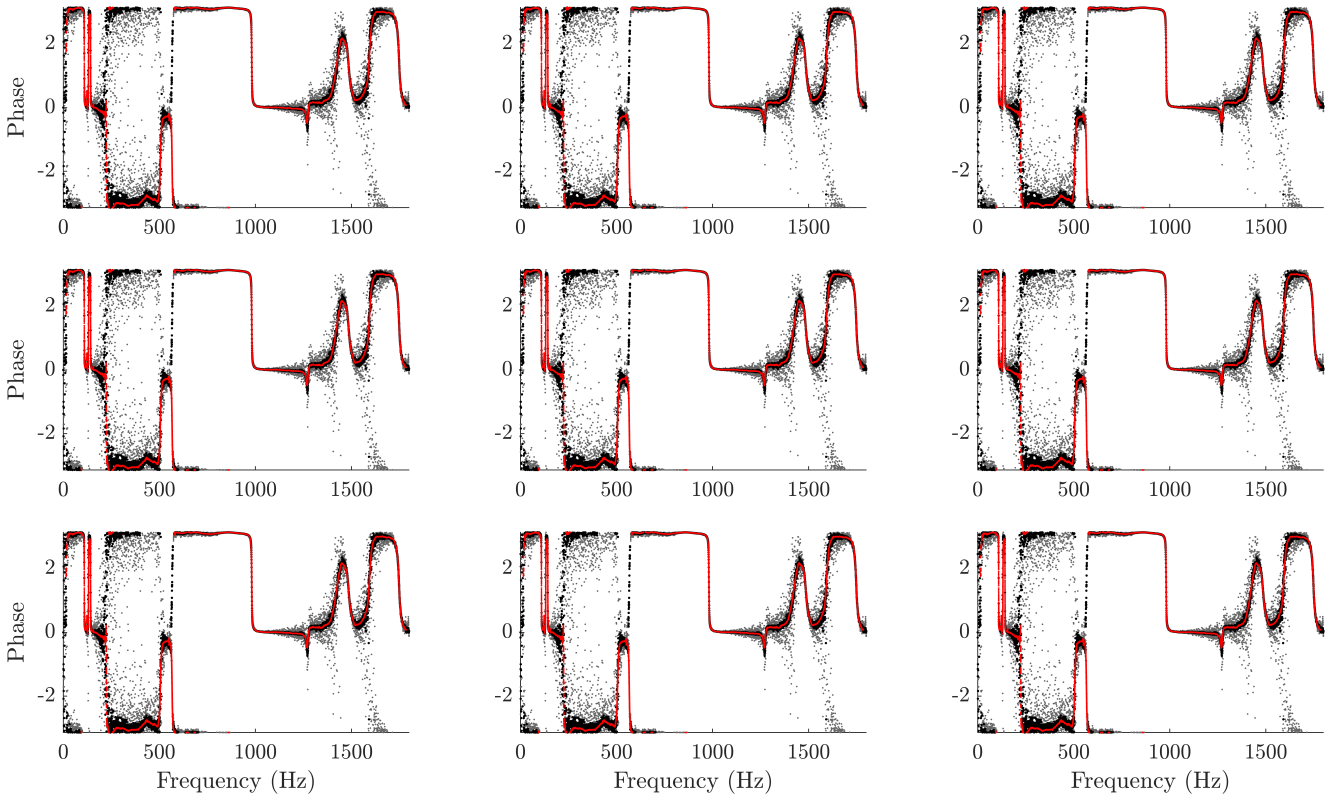

(b)

Figure 6: Estimated FRF (a) magnitude and (b) phase for a three-ouptut sample of the MIMO experimental confguration with 60 seconds of burst-random input. MFRAC values for the entire FRM are 0.785 for H_{SVD} (gray) and 0.868 for LM (red) when compared with the "truth" estimate (black).

5.2 Nonlinear system

This section demonstrates local modeling on a nonlinear assembly (Fig. 8) featuring two beam components combined via a bolted lap joint. The structure is excited by hammer impacts, and responses are measured at eight triaxial accelerometers located along the length of the beam. Because the nonlinear FRM depends on input excitation, all FRFs presented in this section are computed from single impacts. For each impact, 4 seconds of data are recorded. Fig. 9 shows a sample nonlinear resonance profile constructed with $\mathrm{H}_{\mathrm{SVD}}$ and with the local modeling approach. Fig. 10 shows a sample FRF estimated from ten impacts at varying force levels. LM produces single-impact estimation well below the apparent noise floor. Estimation bandwidth for LM is 20 Hz, and transient identification is disabled because the system comes to rest before data collection is stopped, producing minimal leakage. The LM model in Figs. 9 and 10 is manually set to MISO $(3, 2)$.

Figure 8: Nonlinear experiment setup.

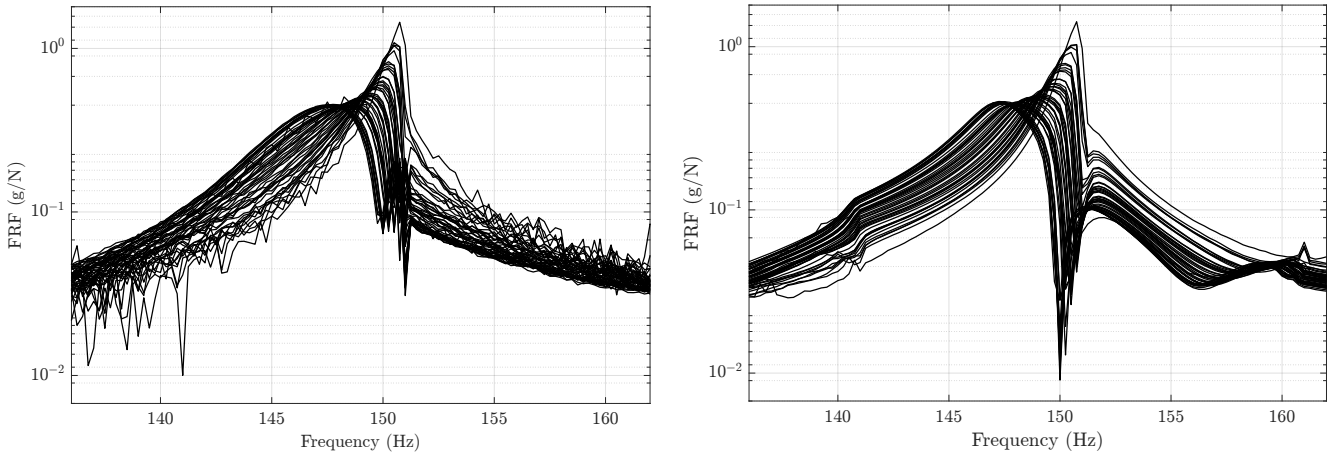

Figure 9: Example of nonlinear characterization using (a) $\mathrm{H}_{\mathrm{SVD}}$ (b) LM with the MISO $(3, 2)$ model (no transient) and a 20 Hz estimation bandwidth.

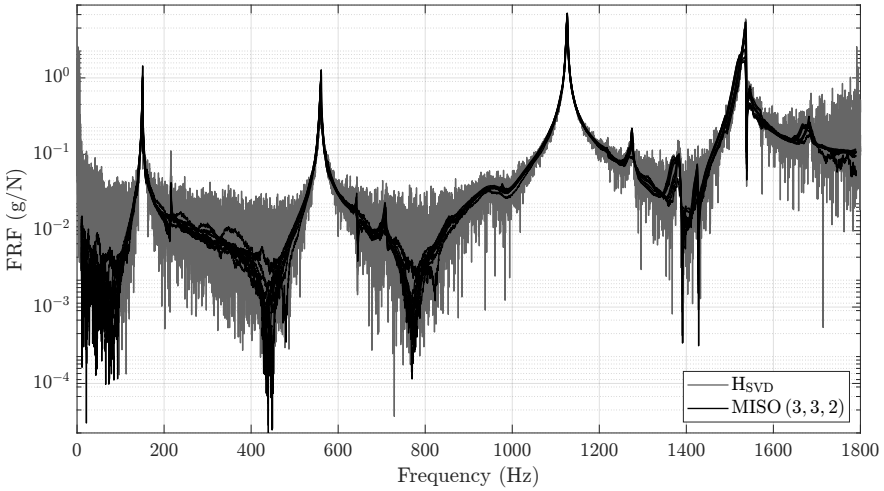

Figure 10: Representative FRF estimated with $\mathrm{H}_{\mathrm{SVD}}$ and LM with the MISO $(3, 2)$ model (no transient) and a 20 Hz estimation bandwidth.

6 Conclusion

This paper reviews the state-of-the-art in local modeling for FRF estimation and proposes updates to make the procedure feasible for dynamic testing. It provides a theoretical framework, including several parameterizations of the local models for MIMO systems. An iterative procedure for optimization of the least-squares objective function is described, and computational improvements for the multi-input, single-output parameterization make local modeling feasible for systems with a large number of output channels. An automatic model-selection procedure for selecting a parameterization and order is proposed and validated. For cases when a model is manually selected, rules of thumb are provided to help the analyst to choose an appropriate model and estimation bandwidth.

Effectiveness of local modeling is demonstrated in a simulation, a MIMO experiment with random excitation, and a nonlinear experiment with impact excitation. To the authors' knowledge, this work documents local estimation on a MIMO system with the most output channels to date, and it is the first to perform the method on a highly nonlinear mechanical system.

References

[1] Randall J. Allemang, Rohit S. Patwardhan, Murali M. Kolluri, and Allyn W. Phillips. Frequency response function estimation techniques and the corresponding coherence functions: A review and update. *Mechanical Systems and Signal Processing*, 162, June 2022.

[2] Robert D. Blevins. *Formulas for Dynamics, Acoustics and Vibration*. John Wiley & Sons, Ltd, November 2015.

[3] Egon Geerardyn, Mikaya L. D. Lumori, and John Lataire. FRF smoothing to improve initial estimates for transfer function identification. *IEEE Transactions on Instrumentation and Measurement*, 64, October 2015.

[4] Levi H. Manring, John F. Schultze, Sandra J. Zimmerman, and Brian P. Mann. Improving magnitude and phase comparison metrics for frequency response functions using cross-correlation and log-frequency shifting. *Journal of Sound and Vibration*, 539, August 2022.

[5] Allan McQuarrie, Robert Shumway, and Chih Ling Tsai. The model selection criterion AICu. *Statistics & Probability Letters*, 34:285–292, June 1997.

[6] Kevin L. Napolitano. Using singular value decomposition to estimate frequency response functions. *Conference Proceedings of the Society for Experimental Mechanics Series*, 10:27–43, 2016.

[7] B. Peeters, P.Z. Csurcsia, and M. Elkafafy. Advanced frequency response matrix estimation using very short measurements. In *Proceedings of ISMA-USD 2022*, 2022.

[8] Rik Pintelon and Johan Schoukens. *System Identification: A Frequency Domain Approach*. IEEE Press, 2012.

[9] Rik Pintelton, Dries Peumans, Gerd Vandersteen, and John Lataire. Frequency response function measurements via local rational modeling, revisited. *IEEE Transactions on Instrumentation and Measurement*, 70, 2021.

[10] C. Sanathanan and J. Koerner. Transfer function synthesis as a ratio of two complex polynomials. *IEEE Transactions on Automatic Control*, 8:56–58, January 1963.

[11] G. Schmidt and A. Tondl. *Non-linear Vibrations*. Cambridge University Press, 1986.

[12] Ka Veng Yuen. *Bayesian Methods for Structural Dynamics and Civil Engineering*. John Wiley & Sons, 2010.

[13] Ka Veng Yuen, Lambros S. Katafygiotis, and James L. Beck. Spectral density estimation of stochastic vector processes. *Probabilistic Engineering Mechanics*, 17:265–272, 2002.

[14] Robbert Voorhoeve, Annemiek van der Maas, and Tom Oomen. Non-parametric identification of multivariable systems: A local rational modeling approach with application to a vibration isolation benchmark. *Mechanical Systems and Signal Processing*, 105:129–152, December 2018.